CrossMark

Eruptive Solar Prominence at 37 GHz

J. Kallunki[1] · M. Tornikoski[1]

Abstract On 27 June 2012, an eruptive solar prominence was observed in the extreme ultraviolet (EUV) and radio wavebands. At the Aalto University Metsähovi Radio Observatory (MRO) it was observed at 37 GHz. It was the first time that the MRO followed a radio prominence with dense sampling in the millimetre wavelengths. This prompted us to study the connection of the 37 GHz event with other wavelength domains. At 37 GHz, the prominence was tracked to a height of around 1.6 $R_\odot$, at which the loop structure collapsed. The average velocity of the radio prominence was 55 ± 6 km s^{-1}. The brightness temperature of the prominence varied between 800 ± 100 K and 3200 ± 100 K. We compared our data with the *Solar Dynamic Observatory* (SDO)/*Atmospheric Imaging Assembly* (AIA) instrument's 304 Å EUV data, and found that the prominence behaves very similarly in both wavelengths. The EUV data also reveal flaring activity nearby the prominence. We present a scenario in which this flare works as a trigger that causes the prominence to move from a stable stage to an acceleration stage.

1. Introduction

On 27 June 2012, an eruptive solar prominence was observed in the extreme ultraviolet (EUV) and radio wavebands. It was the very first time that this type of a moving radio feature was observed at the Aalto University Metsähovi Radio Observatory (MRO). Similar events have been reported earlier, *e.g.* by Klein and Mouradian (2002), Alissandrakis *et al.* (2013),

✉ J. Kallunki
juha.kallunki@aalto.fi

M. Tornikoski
merja.tornikoski@aalto.fi

[1] Metsähovi Radio Observatory, Aalto University, Metsähovintie 114, 02540 Kylmälä, Finland

Irimajiri *et al.* (1995), and Grechnev *et al.* (2006), but most of their radio observations have been conducted at lower frequencies (≤ 17 GHz) or their observations have been more sparse (Irimajiri *et al.*, 1995). Thus the observation presented in this article is unique in this regard.

Prominences can keep very low temperature plasma ($< 10,000$ K) in their core (Landi and Reale, 2013). Based on Hα and Ca II line observations, Park *et al.* (2013) have reported that the temperature of the prominence core varies between $4000 - 20,000$ K. A stable prominence may persist for a period of some hours up to some months.

Eruptive prominence have been observed at least at EUV, X-ray, Hα, and microwave wavelengths (Chifor *et al.*, 2006; Parenti, 2014), and they are usually associated with solar flares. The thermal insulation, which keeps part of the prominence material neutral so that it is visible in Hα, and the confinement of electrons that emit the radio waves require magnetic fields and make the respective emissions a tracer of the dynamics of ejected magnetic-field structures (Klein and Mouradian, 2002).

In this article we present and discuss an observation of an eruptive solar prominence at the wavelength of 8 mm (37 GHz). This is the very first time that such an event was followed through at 37 GHz, which offers a unique opportunity to compare it with simultaneous data obtained in other wavelength domains, and to study possible connections between the energy bands. We present a comparison of radio data with EUV observations. We also define the brightness temperature and the flux and height profiles of the eruptive radio prominence and compare them to earlier studies. Finally, we propose a scenario to explain how an eruptive radio source arises.

2. Observations

The event started at approximately 07:30 UT and ended at approximately 12:30 UT. During the active state, from about 10:00 UT to about 11:20 UT, this event was also observed at the MRO in Finland at the radio frequency of 37 GHz. The radio observations were conducted with MRO's 14-metre radio telescope. The antenna can produce solar maps with a cadence (time between two consecutive solar maps) as short as 180 seconds at its fastest. The observations used in this work were made with a cadence of approximately eight minutes. The observing frequency was 37 GHz, where the beam size of the telescope is 2.4 arcmin.

The measurements are always scaled relative to the quiet-Sun level (QSL), and the observations remain comparable to each other over a series of solar maps (Kallunki *et al.*, 2012). The QSL is the median temperature of the data samples from the solar disc in the radio maps. The brightness temperature of the QSL at 37 GHz is around 8200 K $\pm$ 500 K (Landi and Chiuderi Drago, 2008), which is used as a reference temperature in this study. This means that the solar radio emission at 37 GHz comes mainly from the chromosphere. The atmospheric conditions were almost perfect during the observing session, which is critical for the ground-based observations. In total, we managed to observe nine solar radio maps during this event, which gives us the possibility to perform a comprehensive analysis of this event.

We wished to compare our radio data with the data from the *Solar Dynamic Observatory* (SDO)/*Atmospheric Imaging Assembly* (AIA) instrument (Lemen *et al.*, 2012) 304 Å channel (extreme ultraviolet, EUV). This specific channel is especially good at showing areas where cooler dense plumes of plasma (*e.g.* filaments and prominences) are located. The characteristic temperature is around 50,000 K in this channel, and therefore it is much higher than the brightness temperature of 37 GHz (8200 K). The emission of AIA 304 Å
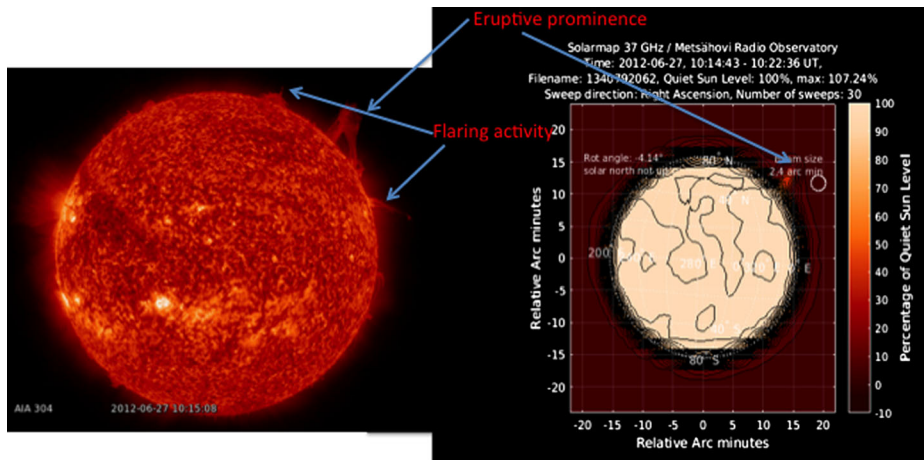
Figure 1 AIA 304 Å image (left) taken at 10:15:08 UT. Solar radio map (right) at 37 GHz, observed at 10:14:43 – 10:22:36 (UT). Locations of the eruptive prominence and flaring activity are marked in the maps. The contours in the radio images represent temperatures in the range of 9.9% to 38.8% of the QSL.

comes from the upper chromosphere and the lower transition region. When interpreting observations of the 304 Å channel, it is important to note that it also includes a contribution from the Si XI line at 303.4 Å (Labrosse and McGlinchey, 2012, and references therein). Thompson and Brekke (2000) calculated the contribution from the Si XI line compared to the He II line, and they estimated that the contribution can be as much as 90% off-limb, but that the He II line dominates in prominences. The prevailing interpretation is that at millimetre wavelengths we can also see influence from material that has much higher temperatures than the brightness temperature (Alissandrakis *et al.*, 2013). Thus the comparison between these two wavelength domains is important.

We also examined the other AIA temperature bands. Some of them showed simultaneous activity, but no other band showed distinguishable prominence loops where the evolution could have been tracked as well as in the AIA 304 Å band. Additionally, some other radio observations (mainly the other solar monitor instruments of the MRO, total flux density observations of the whole solar disc at 11.2 GHz, and broadband spectra of the whole solar disc at 50 – 850 MHz) were examined, but they did not reveal any brightened radio features. Emission in these bands comes from higher regions in the Sun, and they are apparently unrelated to the features discussed in this article.

2.1. EUV and Radio Observations

The radio observations were started at 09:57 UT when the eruptive process was unfortunately already underway according to the AIA images, which show a relatively stable loop structure several hours before the rapid acceleration stage. However, the significant radio eruption was just beginning when our observations were started, and we managed to observe the complete radio acceleration and fading stage.

In Figure 1 a full solar radio map is presented, together with an AIA 304 Å EUV image. The prominence was located in the northern hemisphere and at relatively high latitudes on the east limb.

In Figure 2 we present partial enlargements of the radio maps, centred on the location of the prominence, together with the simultaneously observed SDO AIA 304 Å images.

Figure 2 Temporal evolution of the eruptive prominence: solar radio maps (left) with the contour lines at 37 GHz and AIA 304 Å images (right).
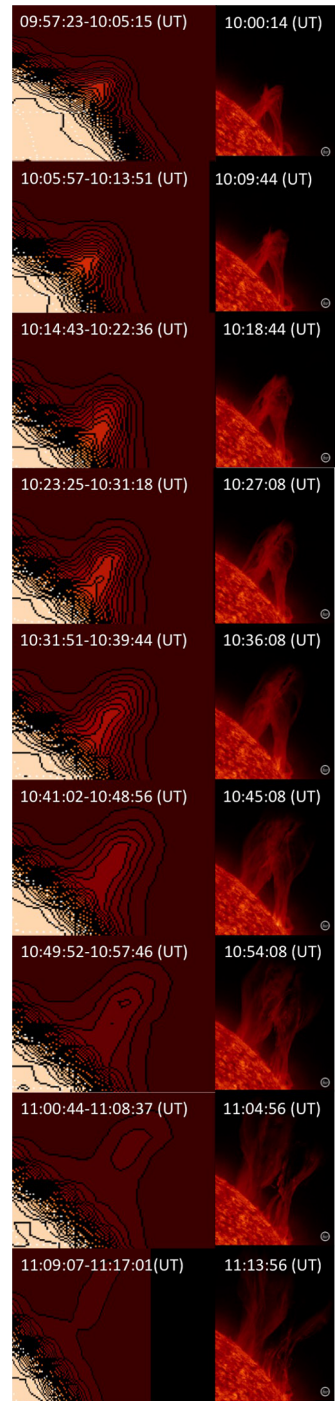
Table 1 Coordinates of the eruptive prominence (top of the prominence loop) observed by radio and AIA. In the first and second columns the locations (latitude and longitude) of the top of the prominence loop at 3 mm are presented. In the third column the maximum temperature (relative to the QSL) of the radio prominence is shown. In the fourth and fifth columns the locations (latitude and longitude) of the top of the prominence loop at 304 Å is presented. The # in the left-hand column is the number of the frame in Figure 2, from top to bottom.

#	Radio long. [rel. arcmin]	Radio lat. [rel. arcmin]	Radio T_B [%]	AIA long. [rel. arcmin]	AIA lat. [rel. arcmin]
1	15.2	14.1	38.8	13.9	14.2
2	15.6	14.1	42.6	14.1	14.6
3	15.8	15.7	41.5	14.2	15.4
4	16.0	15.7	38.9	14.5	16.4
5	16.4	17.4	33.8	15.0	17.3
6	17.4	17.4	24.3	15.0	18.0
7	17.8	17.4	18.1	14.3	18.8
8	17.8	19.0	12.2	14.3	19.0
9	18.0	19.0	9.9	14.8	18.5

The time stamp for each radio map that we obtained is given at the top of each map, and the EUV images included in this figure were selected to represent the midpoint of the time interval when the radio maps were observed, and their time stamps are shown in the figure accordingly. The original EUV data are taken at a cadence of approximately ten seconds.

The observations and their temporal evolution can also be seen as a movie in the electronic supplementary material (or www.metsahovi.fi/~kallunki/Radio_prominence). Because the temporal resolution of the two wavebands is very different, the details of the EUV feature are best viewed in the animation with higher temporal resolution than Figure 2. In Table 1 the coordinates of the prominence-loop outer edge are presented. The edges were selected by visual examination, and the accuracy is determined by the resolution of the radio images. The angular resolution of the radio observations (2.4 arcmin) is lower than that of AIA, which prevents us from determining whether finer-scale loop structures are also present in the radio data. We can only compare the overall structure and the development of the activity between these two wavebands.

In Figure 3 we have calculated data based on the visual examination of Figure 2 and the data collected in Table 1. The data stream of these nine points yields the height profile (upper-left panel of Figure 3) and the speed profile (upper-right panel) of the prominence in each waveband, together with the radio brightness temperature (lower-left panel) and the radio flux and temperature profile (lower-right panel). The EUV data were selected to match the tip of the prominence loop in each image; the radio data used for this were selected to match the brightest feature in each map.

For the whole acceleration stage, the prominence loop (four uppermost image rows in Figure 2) was expanding and the loop structure stayed in a compact form. At this stage the features at the two frequency bands are relatively co-spatial. Simultaneously, the radio source is moving away from the solar disc to the corona. The temperature of the radio source remains fairly constant over this period (Figure 3, lower-right plot). The loop structure starts to collapse after around 10:30 UT (Figure 2, fifth image row and afterwards). Now the EUV emission region expands and the tip moves away from the direction of the radio feature. This also has an influence on the structure of the radio source. The temperature of the radio source starts to decrease rapidly and the whole radio source starts to fade away. In the last image row, we can barely see the radio source (11:09:07 – 11:17:01 UT). Thus the whole eruptive radio prominence did not last more than 70 – 80 minutes. It is very clear that the microwave and the 304 Å EUV emission have a tight connection to each other during this event.
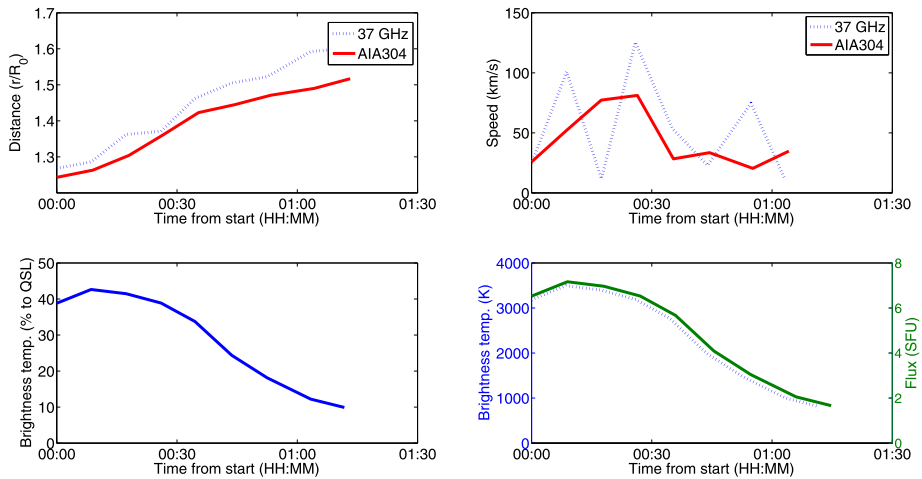
Figure 3 Upper-left panel: height profile of the eruptive prominence (both radio and EUV). Upper-right panel: speed profile of the eruptive prominence (both radio and EUV). Lower-plot panel: temperature profile (percent relative to QSL) of the eruptive prominence (radio). Lower-right panel: brightness temperature and flux profile of the eruptive prominence (radio). The start time of these plots is when the first solar radio map was observed: 09:57:23 UT.

2.2. Temperature and Flux and Height Profiles

We managed to track the prominence to a distance of 1.6 $R_\odot$ before the prominence structure collapsed. Both observations (radio and EUV) show that the height increases almost linearly (Figure 3, upper-left plot). Gopalswamy *et al.* (2003) have made an extensive statistical study of the properties of prominence eruptions in microwaves, and they have found that the average height is 1.35 $R_\odot$. Thus, the event analysed here is far higher than the average eruptive prominence. In Figure 3 (upper-right plot) we show the velocity profile of the prominence. The irregularity in the radio velocity profile is mainly caused by the inaccuracy of the radio observations (relatively large beam size). However, the average velocity will give more reliable information about the speed. The average speed for the radio feature in this case is estimated to be 54 ± 6 km s^{-1} and for the EUV feature it is 44 ± 3 km s^{-1}. This is very close to the statistical average speed of 56.0 km s^{-1} (Gopalswamy *et al.*, 2003). In this respect, the analysed prominence was very typical.

The maximum brightness temperature of the prominence varies between 800 K and 3200 K with a temperature resolution of approximately 100 K (Figure 3, lower-right plot). Previous studies have shown that the brightness temperature of eruptive prominences can vary between 4500–6000 K at a frequency of 17 GHz and between 6500–7500 K at a frequency of 5.7 GHz (Grechnev *et al.*, 2006). Additionally, Irimajiri *et al.* (1995) have reported that the brightness temperature of eruptive prominences is 2500–5300 K at 36 GHz, 780 K at 89 GHz, and 600–1200 K at 110 GHz. The analysed prominence, with its maximum brightness temperature of 3200 K, is rather close to the values reported earlier. The brightness temperature [T_B] can also be converted into the radio flux [S_{sfu}] as

$$S_{\text{sfu}} = 7.22 \times 10^{-11} \nu^2 \rho^2 T_B, \tag{1}$$

where ν is the observing frequency (in GHz) and ρ is the beam size (in arcsec). The maximum flux of the eruptive prominence is 7.2 ± 0.1 SFU (Figure 3, lower-right plot). Grechnev

et al. (2006) reported a prominence from 4 September 2000, and their calculations showed that the maximum flux was 6 SFU. Another event that they report was on 14 January 2001, and the flux varied during that event from 10 to 18 SFU.

2.3. Flaring Activity

Interestingly, there was also some flaring activity during the eruptive prominence. This can be seen in the AIA 304 Å movie and in Figure 1. The solar flares (and their positions) are marked in the AIA image. The second flare was quite close to the eruptive prominence (marked with an arrow in Figure 1, located at the right below the eruptive prominence), and it was also active during the prominence. The flare next to the prominence starts to rise when the prominence moves to the acceleration stage. The flare is active until the prominence loop collapses.

This particular flare was detected neither at the millimetre wavelengths (see the solar radio map movie) nor at lower radio frequencies, and its possible effect on the observed radio prominence remains unclear. Overall, however, the Sun was in a very active state in the radio bands between 25 June and 29 June, 2012. The MRO observed and tracked several active regions (AR 11512, AR 11513, and AR 11515) during that period, and they also produced numerous X-ray flares.

3. Results and Conclusions

For the first time, we observed an eruptive prominence with high-cadence sampling at 37 GHz. When we compared it to previous studies, its speed and flux were typical of such prominences, but the observed height was higher (1.6 $R_\odot$) than the average (1.35 $R_\odot$). The millimetre-wavelength observations coincide accurately with 304 Å EUV observations.

Flaring events in the EUV were also observed during the same period. With only this set of observations, no conclusive statements can be made about their connections, but below we propose a scenario to explain how the change in a prominence structure could be triggered by a flaring event, and how the features observed in the radio and EUV domains can be connected. Previously, Karlický and Shibasaki (2002) have also suggested that some other feature works as a trigger for an eruptive prominence.

  i) A quiet/stable prominence is visible.
 ii) A flare arises next to the prominence.
iii) The flare next to the prominence works as a trigger that causes the prominence to move from a stable stage to an acceleration stage, and the prominence loop starts to expand.
 iv) A loop raises cooler plasma from the chromosphere, which can also be observed at millimetre wavelengths.
  v) A radio source arises.
 vi) The loop structure eventually becomes unstable, collapses, and loses its energy.
vii) The radio source disappears soon after the collapse of the prominence loop structure.
viii) The prominence also slowly fades away.

Disclosure of Potential Conflicts of Interest   The authors declare that they have no conflicts of interest.

References

Alissandrakis, C.E., Kochanov, A.A., Patsourakos, S., Altyntsev, A.T., Lesovoi, S.V., Lesovoya, N.N.: 2013, *Publ. Astron. Soc. Japan* **65**, S8. DOI. ADS.

Chifor, C., Mason, H.E., Tripathi, D., Isobe, H., Asai, A.: 2006, *Astron. Astrophys.* **458**, 965. DOI. ADS.

Gopalswamy, N., Shimojo, M., Lu, W., Yashiro, S., Shibasaki, K., Howard, R.A.: 2003, *Astrophys. J.* **586**, 562. DOI. ADS.

Grechnev, V.V., Uralov, A.M., Zandanov, V.G., Baranov, N.Y., Shibasaki, K.: 2006, *Publ. Astron. Soc. Japan* **58**, 69. DOI. ADS.

Irimajiri, Y., Takano, T., Nakajima, H., Shibasaki, K., Hanaoka, Y., Ichimoto, K.: 1995, *Solar Phys.* **156**, 363. DOI. ADS.

Kallunki, J., Lavonen, N., Järvelä, E., Uunila, M.: 2012, *Balt. Astron.* **21**, 255. ADS.

Karlický, M., Shibasaki, K.: 2002, In: Wilson, A. (ed.) *Solar Variability: From Core to Outer Frontiers* **SP-506**, ESA, Noordwijk, 657. ADS.

Klein, K.-L., Mouradian, Z.: 2002, *Astron. Astrophys.* **381**, 683. DOI. ADS.

Labrosse, N., McGlinchey, K.: 2012, *Astron. Astrophys.* **537**, A100. DOI. ADS.

Landi, E., Chiuderi Drago, F.: 2008, *Astrophys. J.* **675**, 1629. DOI. ADS.

Landi, E., Reale, F.: 2013, *Astrophys. J.* **772**, 71. DOI. ADS.

Lemen, J.R., Title, A.M., Akin, D.J., Boerner, P.F., Chou, C., Drake, J.F., *et al.*: 2012, *Solar Phys.* **275**, 17. DOI. ADS.

Parenti, S.: 2014, *Living Rev. Solar Phys.* **11**, 1. DOI. ADS.

Park, H., Chae, J., Song, D., Maurya, R.A., Yang, H., Park, Y.-D., *et al.*: 2013, *Solar Phys.* **288**, 105.

Thompson, W.T., Brekke, P.: 2000, *Solar Phys.* **195**, 45. DOI. ADS.